A Consistent Picture of the Actin Filament Related to the Orientation of the Actin Molecule

WALTER E. FOWLER and UELI AEBI
Department of Cell Biology and Anatomy, Johns Hopkins University School of Medicine, Baltimore, Maryland 21205

ABSTRACT We show that freeze-dried actin filaments which have been rotary shadowed with a light coat of platinum appear very similar in morphology and width to negatively-stained filaments. The addition of a thicker coat of platinum to such preparations gives the actin filaments a different morphology and width, which are similar to those of the rotary-shadowed, quick-frozen filaments described by Heuser and Kirschner (*J. Cell Biol.* 1980, 86:212–234). The consistent view of the actin filament presented here, particularly its 7–8-nm width, can be interpreted in terms of the overall orientation of the actin subunit in the actin filament.

Although the importance of actin in the cell has long been recognized, only in the past few years have relatively high resolution structural data about the actin molecule become available. Recent studies of crystalline forms of actin alone (1, 2) or of actin-DNase I complexes (3, 27) have shown that actin is an elongated globular molecule with linear dimensions of ~5–7 × 4 × 3 nm. To fully exploit these three-dimensional molecular models of actin (2, 3) in functional terms, it is necessary to relate them to the actin filament. Since neither of the crystalline forms seem to be built directly from actin filaments (1, 3) and since existing filament reconstructions do not allow unambiguous tracing of the actin subunit within them (2, 4–6), the orientation of these molecular models within the actin filament remains speculative.

Two different orientations have been proposed recently. In one (1–3), the "long axis" of the molecule (i.e., 5–7 nm)[1] is oriented parallel to the filament axis and in the other (7, 8), these two axes are nearly perpendicular to each other. Although actin filament models having the correct helical parameters (9, 10) can be built using either the parallel or the perpendicular molecular orientation, the resulting filament models have widths of 6–8 nm (2, 3) and at least 9.5 nm (7, 8), respectively. Although knowledge of the true filament width should be sufficient to distinguish between these two possible orientations, width values in the literature—and indeed the overall morphology of the filament itself—seem to depend strongly on the method used to prepare the filaments for examination in the electron microscope.

Published width measurements of negatively stained actin filaments range from 6 to 8 nm (4, 5, 9, 11) and are therefore consistent with the parallel molecular orientation. However, since the width of a negatively stained structure is determined by its stain exclusion profile, the resulting value may be an underestimate. In contrast, quick-frozen/rotary shadowed actin filaments have yielded uncorrected widths of at least 9.5 nm (12, 13), which would seem to support the perpendicular molecular orientation (7, 8); moreover, such filaments display a distinctive morphology that appears inconsistent with that seen in negative stain (12, 13). However, the thickness of the metal coat can account for a substantial fraction of the apparent particle dimensions in shadowed preparations and can differentially alter the appearance of structural features.

To try to resolve these ambiguities, we have systematically investigated the effects of shadow angle and metal replica thickness on the width and appearance of freeze-dried actin filaments. We report here that lightly rotary shadowed actin filaments are very similar in width and appearance to negatively stained filaments, thus providing a consistent view of the actin filament that supports the parallel orientation of the actin molecule within it.

MATERIALS AND METHODS

Actin Filaments: Column-purified rabbit skeletal muscle actin was prepared as described (1). G actin, at 0.2 mg/ml, was polymerized for at least 30 min at room temperature by adding 2.5 mM $MgCl_2$.

Specimen Preparation: For both negative staining and freeze-drying, 5 μl-samples of a 1:10 dilution of F actin in 2.5 mM $MgCl_2$ were applied to glow discharged, carbon-coated grids for 1 min. After removing excess sample, grids were washed for 10 s by applying a drop of distilled water, blotting with filter paper, and either negatively staining with 0.75% uranyl formate, pH 4.25,

[1] In the case of the actin model determined from crystalline actin sheets (2), we define the long axis of the molecule as being parallel to the 5.6-nm unit cell vector. Since the long axis of the actin models determined from actin-DNase I crystals appear to be at least 6.5 nm (3, 27), the "long axes" of the two types of molecular models may not be exactly parallel. This point is discussed in detail in reference 2.

THE JOURNAL OF CELL BIOLOGY · VOLUME 97 JULY 1983 264–269
© The Rockefeller University Press · 0021-9525/83/07/0264/06 $1.00

or freezing by plunging the grid into liquid nitrogen. Frozen samples were loaded onto a brass table as described (14, 28), covered with a copper cap, and transferred to a precooled Balzers 400 freeze-etching (Balzers, Hudson, NH) unit via a counterflow loading device (14). These samples were dried for 1 h at −100°C and were then unidirectionally or rotary shadowed from a platinum/carbon electrode in an electron beam evaporation source. Thickness of the metal replica was monitored using a quartz crystal thin film monitor (Balzers). The shadowed specimens were stabilized by depositing a thin film of pure carbon from directly above before venting the unit.

Electron Microscopy and Filament Width Measurements: Specimens were examined in a Zeiss EM10C electron microscope. Magnification was calibrated using negatively stained catalase crystals (15). All micrograph negatives of shadowed specimens were photographically reversed before printing, with care taken to preserve the correct handedness. As a consequence, shadows appear dark (Fig. 2).

Width measurements were made either on prints enlarged to at least × 150,000 or using a Nikon optical comparator (Nikon, Inc., Instrument Div., Garden City, NY), on which the micrographs were projected at × 920,000.

Computer Modeling: The filament shown in Fig. 4 was modeled by Dr. R. J. Feldmann (National Institutes of Health) and the authors using an Evans and Sutherland interactive graphics display system. Briefly, the surface of the three-dimensional model of the actin subunit as determined from crystalline actin sheets (2) was approximated by 50 interpenetrating spheres of various radii. In generating the filament model from these subunits, the 5.6-nm axis of the molecular model was kept parallel to the filament axis. The distance of this axis from the filament axis and the angular orientation of the subunit around this axis were chosen to give the best fit with an actual filament model computed from polylysine-induced actin filament paracrystals as we have described elsewhere (2).

RESULTS

Negatively Stained Actin Filaments

Negatively stained actin filaments (Fig. 1 *a*) appear to consist of two strands of approximately globular subunits helically wound around each other (4, 5, 9). The sense of the two, long pitch (i.e., ~74 nm) helices has been shown by unidirectional shadowing to be right handed (16; [Fig. 2]). If negatively stained filaments (e.g., Fig. 1 *a*) are viewed obliquely along the filament axis, a more or less regular variation in the width of the filament with a periodicity of ~37 nm can often be observed along its length. This corresponds to positions along the filament where the two long pitch helices lie next to one another on the substrate (wide) and where they crossover each other (narrow). Although it has been stated that the appearance of the crossovers distinguishes filament models built using the perpendicular and parallel molecular orientations (7, 8), the prominence of filament crossovers in typical negatively stained preparations (e.g., Fig. 1 *a*) is variable, even along a single filament. In fact, the appearance of negatively stained actin filaments can vary considerably both with respect to morphology and width (see below). This is probably due to the effects of spread flattening and/or collapse during specimen preparation (17 [Fig. 3 *a*]), the retraction of stain during irradiation (18), and the inherent random variable twist of the actin helix (19), all of which combine to distort and deform the actin helix. It is therefore difficult to decide objectively what is the "true" appearance of a negatively stained actin filament.

Freeze-dried Actin Filaments

Freeze-drying has been widely used to reduce the effects of specimen collapse that usually occurs during simple air-drying (14, 17). Such preparations are most often examined after unidirectional or rotary shadowing with a heavy metal. The resulting images often depend critically upon the shadowing angle and the thickness of the metal replica (20, 21). Lightly shadowed actin filaments (Fig. 1 *b*) were 7.5–8.5 nm wide and appeared similar to negatively stained filaments (Fig. 1 *a*), particularly with regard to the modulation in width. The right-handed sense of the two long pitch helices and the indication of crossovers at regular intervals could be seen clearly in this rotary shadowed preparation (Fig. 1 *b*, look at a glancing angle). In contrast, identical actin filament preparations that were rotary shadowed with approximately four times the amount of metal from a slightly higher angle (Fig. 1 *c*) appeared more similar to the images of rotary-shadowed, quick-frozen filaments in the literature (12, 13): They were nearly uniform in width (in Fig. 1 *c*, 10–11 nm), had less pronounced crossovers and, although the two long pitch helices could still be seen in favorable cases (Fig. 1 *c*, look at a glancing angle), the increased thickness of the metal replica made this feature less prominent.

Like the width, the appearance of the filament substructure varied considerably with the thickness of the metal coat. As the thickness of the metal replica was increased (compare Fig. 1 *b* with Fig. 1 *c*), the most distinctive feature of freeze-dried, rotary-shadowed filaments became a prominent, near-transverse striation that repeated every 5.9 nm along the length of the filament [8, 12, 13]. It has been suggested that this feature is a manifestation of the shallow, left-handed "genetic" helix of the actin filament that has a 5.9-nm pitch (13; [Discussion and Fig. 4]). Although both lightly (Fig. 1 *b*) and heavily (Fig. 1 *c*) shadowed filaments exhibited this feature, the lightly shadowed filaments also showed substantial variation in substructure along and perpendicular to the filament axis (Fig. 1 *b*), much like negatively stained filaments (Fig. 1 *a*).

The selective enhancement of certain structural features such as the 5.9-nm repeat by shadowing is clearly demonstrated in Fig. 2, which shows actin filaments shadowed unidirectionally. Filaments at different azimuths relative to the shadowing direction (Fig. 2, arrow) displayed different features: filaments nearly parallel to the shadowing direction show the long pitch helix and the 5.9-nm repeat, filaments perpendicular to this direction show little substructure and filaments at intermediate angles show primarily the 5.9-nm repeat. It is very likely that some of these structural features are enhanced or even generated by metal decoration (22). Since a rotary-shadowed filament is effectively shadowed at all azimuths, strongly contrasted features are superimposed onto weakly contrasted ones. Consequently, a rotary-shadowed structure with a metal coat may display surface features weighted quite differently from the original appearance, i.e., in negative stain. In the case of the actin filament, certain features such as the 5.9-nm repeat were selectively emphasized by unidirectional shadowing at certain azimuths (Fig. 2) and may be overemphasized relative to other features (e.g., the right-handed long pitch helices) in rotary shadowed preparations, particularly when the metal replica was relatively thick as in Fig. 1 *c*. The relatively uniform width of heavily shadowed filaments (compare Fig. 1 *c* with Figs. 1, *a* and *b*) may be due to metal decoration (22) and/or to the varying height of the structure above the specimen support: the increased height of the filament at the cross-overs may have caused accumulation of more metal, thus making these regions appear almost as wide as stretches where the two long pitch helices lay side-by-side. As a consequence, the filament would show a more uniform width than is seen in negatively stained filaments.

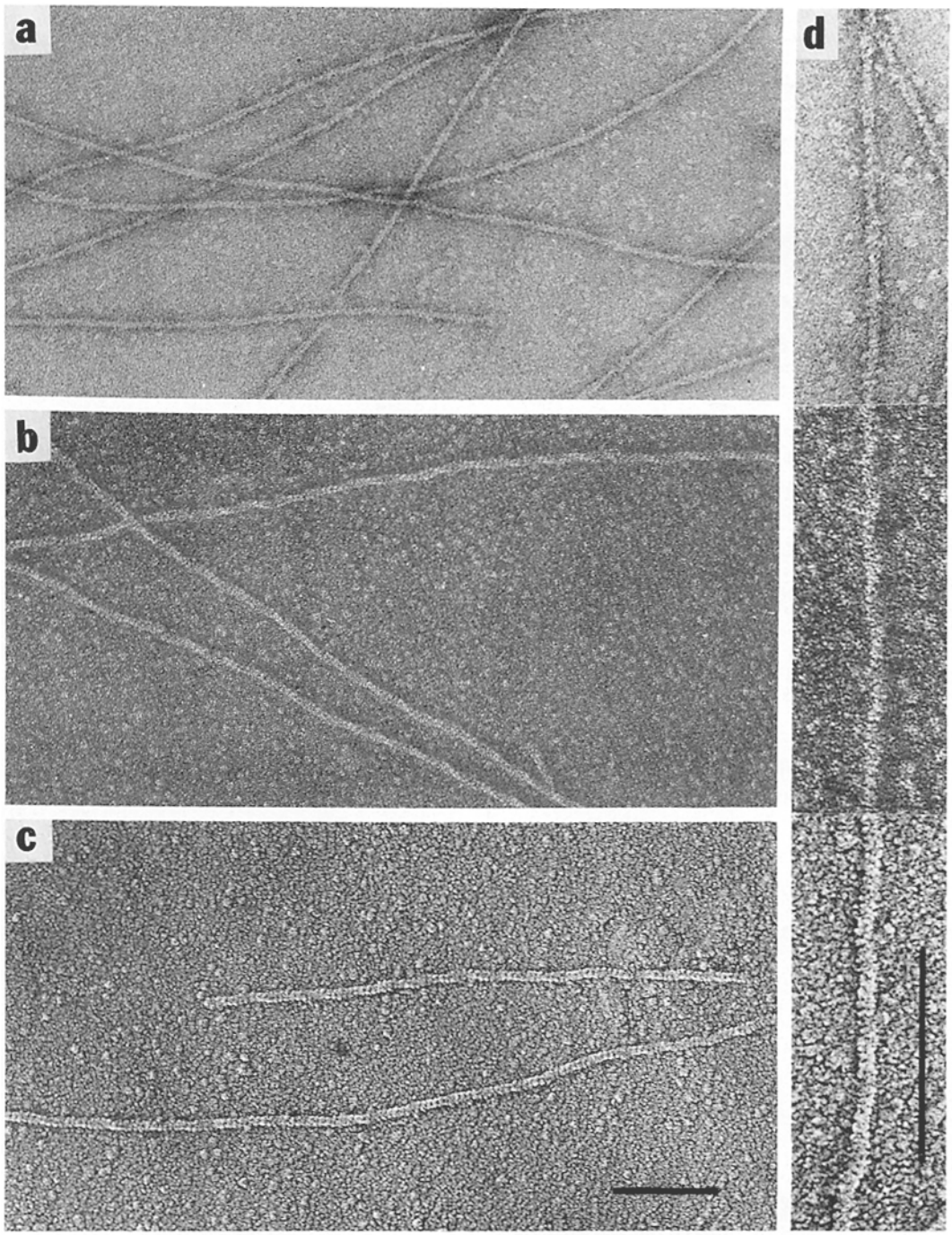

FIGURE 1 Electron micrographs of actin filaments prepared by negative staining (a) or by freeze-drying followed by rotary shadowing with different amounts of platinum (*b* and *c*). For comparison of the filament widths, a composite filament (*d*) has been constructed from lengths of the filaments shown in *a*, *b*, and *c*. The specimen in c was rotary shadowed with approximately four times the amount of platinum/carbon that was used for the specimen in *b*; the elevation angle for shadowcasting was ~15° in *b* and ~25° in c. Compare the appearance of filament crossovers (see text) in the three different preparations by sighting along the filament axis at an oblique angle. Bars, 100 nm. × 158,000 (*a–c*); × 300,000 (*d*).

Determination of Actin Filament Width

Determination of the absolute width of the actin filament is complicated by the various steps involved in preparing the specimen for visualization in the electron microscope, such as adsorption, drying, staining or shadowing, radiation damage, etc. (17). Measurement of the center-to-center spacing of filaments in side-to-side aggregates (e.g., paracrystals) might be expected to give more reliable values than measurement of isolated filaments; in such cases relatively low values (e.g., 6 nm [4, 23]) were obtained. However, if adjacent filaments are laterally interdigitated or are not lying in a plane perpendicular to the electron beam, as is the case in hexagonally packed filament arrays (24), measurement of interfilament distance will yield an underestimated filament width. A more straightforward way of determining filament width is to use "single-layered arrays" of filaments, negatively stained examples of which are shown in Fig. 3*a*. In such arrays, the

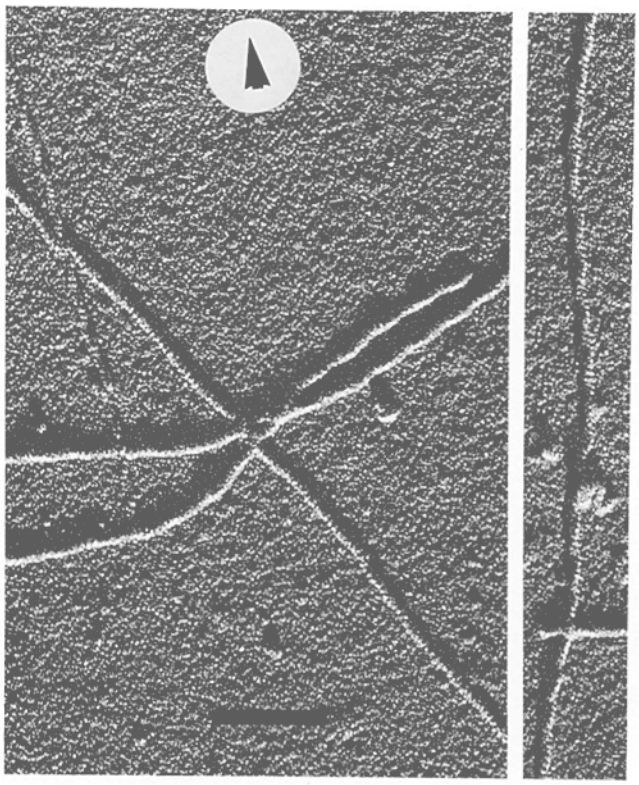

FIGURE 2 Electron micrographs of freeze-dried actin filaments unidirectionally shadowed with platinum/carbon at an elevation angle of ~15°. Note that different structural features are emphasized in actin filaments lying at different azimuths relative to the shadowing direction. The shadowing direction is indicated by the arrow. Bar, 100 nm. × 150,000.

crossovers of adjacent filaments can be in register (top) or more or less random (bottom). Although adjacent filaments that are in register are probably in contact with each other, the prominent dark stain line between adjacent filaments indicates that interdigitation in this array was minimal. In contrast, filaments in the array shown in the bottom of Fig. 3*a* probably made only occasional contact with each other and are almost certainly spread flattened (17) to some extent. Measurement of the center-to-center spacing in single-layered arrays yielded an average value of 7.9 nm and ranged from 6.9 nm for filaments in contact (e.g., Fig. 3*a*, top) to 8.5 nm for partially flattened filaments (e.g., Fig. 3*a*, bottom). Width measurements of isolated filaments in negatively stained preparations always yielded a range of values from 6–8 nm and averaging ~7.0 nm (data not shown). This variability is caused by distortion of the actin helix by a number of factors (see above; [17–19]).

In contrast, the widths of freeze-dried shadowed filaments, although relatively constant within a preparation, have been shown to vary with the thickness of the metal replica (Fig. 1, *b* and *c*); the same has been shown to be true in freeze-etched shadowed preparations (11). Due to metal decoration (22), determination of the correction factor to be applied to measurements for the thickness of the metal coat is not straightforward (13). A novel method of correcting for the replica thickness, which was suggested to us by Dr. John Heuser (Washington University), is shown in Fig. 3*b*. This method depends on the assumption that the thickness of the metal coat that accumulates around two laterally associated filaments lying flat on the support film is the same as that which accumulates around a single filament; thus, by subtracting the uncorrected width of a single filament from that of the "doublet", one should obtain the corrected width for a single filament. The resulting value for the corrected filament width was ~7.7 nm in the case of the two doublet/singlet pairs in Fig. 4. Obviously, this method will yield an underestimate if

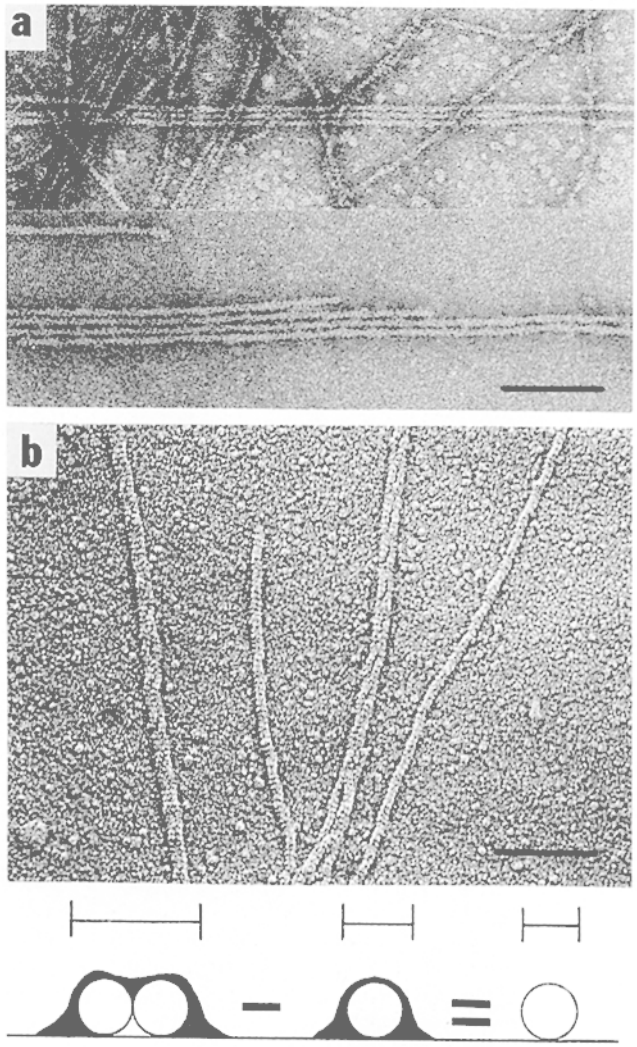

FIGURE 3 Methods of estimating the true width of actin filaments in negatively stained (*a*) and rotary-shadowed (*b*) preparations. (*a*) Examples of 'single layered arrays' that can be found to some extent in filament preparations and in Mg^{++}-induced or polylysine-induced (23) paracrystal preparations. The average center-to-center spacing of filaments in such structures ranges from 6.9 nm where adjacent filaments are in register (i.e., in contact; *top*) to 8.5 nm where filaments are partially 'spread flattened' ([17] *bottom*). (*b*) Illustration of a method suggested to us by Dr. John Heuser to correct filament width measurements for the thickness of the platinum replica. The micrograph, which is from a rotary shadowed preparation such as that shown in Fig. 1 *c*, contains stretches where two laterally associated filaments are lying flat on the support film, as well as stretches of single filaments. As shown in the diagram (*bottom*), such 'doublets' and 'singlets' probably accumulate the same amount of platinum during rotary shadowing. If the widths of both such structures are measured consistently, their difference should equal the width of a single filament corrected for the thickness of the metal replica; this value averages 7.7 nm in the cases shown. It should be noted that this method will yield an accurate width value only if there is no substantial interdigitation between adjacent filaments (see text). Bars, 100 nm. × 138,000 (*a* and *b*).

laterally associated filaments are significantly interdigitated. However, the value obtained is consistent with the interfilament distances (i.e., 7.9 nm on average) measured in negatively stained single-layered arrays (e.g., Fig. 3*a*).

It is reasonable to assume that a thinner metal coat (e.g., Fig. 1*b*) would allow more accurate measurement of filament width in cases where no correction for metal thickness was made. By examining unstained preparations of freeze-dried actin filaments in the scanning transmission electron microscope (STEM), one can obviate the need for such correction altogether. Such filaments appeared well preserved in dark field micrographs (M. K. Reedy, Duke University, personal communication), although definition of the outer filament boundary was somewhat ambiguous. Nevertheless, preliminary measurements by one of us (W. E. Fowler) using micrographs supplied by Dr. M. K. Reedy yielded an average filament width of 7.5 nm. A quantitative study of actin filament width using the STEM is presently being conducted by Dr. Reedy.

DISCUSSION

In spite of the difficulty of obtaining an absolute measure of filament width, the trend of our experimental results is quite clear. It is perhaps best illustrated in the composite filament shown in Fig. 1*d*, where filament widths in three different preparations are compared: The reduction in metal replica thickness brought the filament width in rotary-shadowed preparations much closer to that obtained with negatively stained filaments. Since radial expansion of the filament owing to collapse, adsorption, or metal thickness would most likely outweigh any radial shrinkage, the more accurate width value was probably 7–8 nm, which agrees very well with values obtained by x-ray diffraction of actin filaments in solution (25) or in pellets (26). Given the known size and shape of the actin subunit (1–3), the orientation of its long axis (i.e., 5–7 nm; see footnote 1) within a filament of this width must be closer to parallel than to perpendicular, as described above (2, 3, 8).

The intermolecular contacts that occur in crystalline actin-containing structures (1–3) may offer further clues as to the orientation of the actin molecule in the actin filament. Polar "strands" of actin molecules with their long axes aligned parallel to the strand axis, i.e. having a 5.6-nm intermolecular repeat, run parallel to the 5.6-nm lattice vector in gadolinium-induced actin sheets; due to the presence of a twofold axis of symmetry, adjacent strands in the sheet plane have opposite polarity (1). Both the polar nature of these strands and their axial repeat of 5.6 nm are consistent with the characteristics of each of the two long pitch helices of the actin filament. Although the head-to-tail contact may be similar in the sheet and filament strands, the lateral contacts between strands in the sheet and in the filament must be distinct because of differences in the stagger and polarity of adjacent strands in the two structures (1). In contrast, the presence of a two-fold screw axis relating adjacent actin molecules in crystals of actin-DNase I complexes with an intermolecular repeat of 5.6 nm along the constituent "strands" may suggest that this crystal is built from slightly underwound actin filaments (3, 8). However, since the resulting filaments would be 12 nm in width, these authors decided that the molecular arrangement in these crystals is probably different from that in the filament (3). It is noteworthy that when the actin molecule determined from these co-crystals is oriented so that its long axis is parallel to the filament axis, the resulting filament model is about 8 nm wide (3).

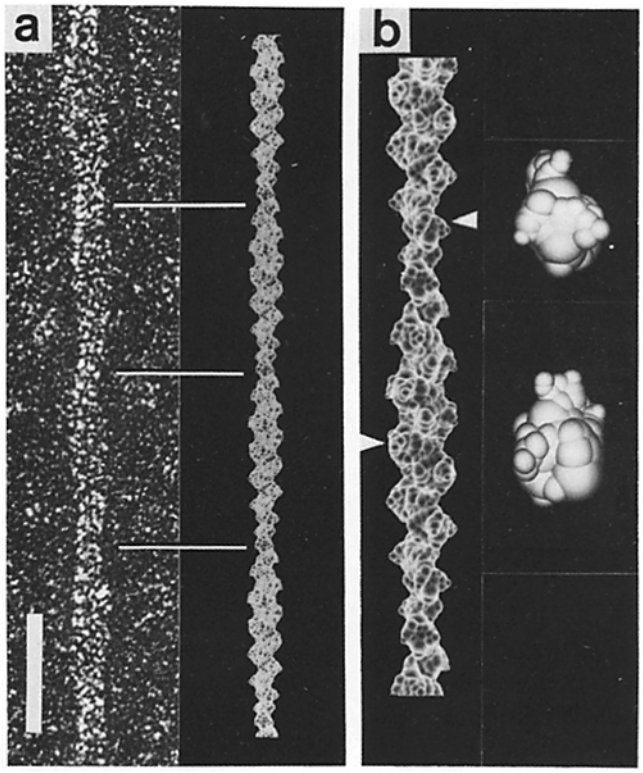

FIGURE 4 Comparison of the morphology of a freeze-dried/rotary-shadowed actin filament similar to those shown in Fig. 1*b* with a filament model built from a three-dimensional molecular model of the actin molecule (12). In this filament model (i.e., the 'best fit' model of reference 2), the long axis of the molecular model is oriented parallel to the filament axis (see text). Common features seen in both the micrograph (*a*, *left*) and the model (*a*, *right*) are the regular variation in width along the length of the filament, the appearance of the right-handed long pitch helices, and the presence of the 5.9-nm pitch of the left-handed genetic helix, which is seen in rotary-shadowed filaments as a prominent cross striation (8, 12, 13). In *b*, part of the filament model in *a* is shown at twice the magnification; two actin 'subunits' have been extracted from the filament model at the positions indicated (arrowheads); each is shown with the same orientation that it had in the filament but at five times the magnification of *a*. Note that the long axis of each subunit in the filament model is oriented parallel to the filament axis. The two extracted subunits shown are related to each other by rotation of 90° about a vertical axis parallel to the filament axis. Bar in *a*, 25 nm. × 632,000 (*a*).

In Fig. 4*a*, the appearance of a freeze-dried/rotary shadowed filament is compared with a filament model generated from a three-dimensional model of the actin molecule (2) using the parallel molecular orientation. Although this filament model was originally built to fit the molecular model of actin (2) to a three-dimensional reconstruction of an averaged negatively stained actin filament obtained from polylysine-induced paracrystals (2, 23), there is also good qualitative agreement between this model and the gross morphology of this rotary shadowed filament (Fig. 4*a*), such as the width modulation and the appearance of the two right-handed long-pitch helices. The concentration of mass in the model along the left-handed genetic helix (9, 10) can easily be related to the 5.9-nm cross striation that is emphasized by rotary shadowing and gives rise to a strong sixth layer line seen in

diffraction patterns of actin filaments (8; [our unpublished results]). The subunit orientation used here, i.e., with the long axis of the molecule parallel to the filament axis, is seen more clearly in Fig. 4*b*, where subunits have been extracted from two points along the length of the filament model and are shown enlarged.

There is still some uncertainty about the exact angular orientation of the actin subunits about their long axes (i.e., in the radial plane)—at least one alternative fit exists (2). However, the correlation presented here of the well-known negatively stained image of the actin filament with the newer rotary-shadowed image provides evidence for the validity of existing filament models (e.g., 2, 5, 6). Our interpretation of this consistent picture of the actin filament in terms of the orientation of the actin subunit is a first step in establishing the localization of functional binding sites on the actin molecule for the many regulatory proteins that mediate the many important interactions of the actin filament in muscle and nonmuscle cells.

We thank Drs. Tom Pollard and P. R. Smith for critical reading of this manuscript and Drs. David DeRosier and John Heuser for preprints of references 8 and 13, respectively. This work was supported by a Muscular Dystrophy postdoctoral fellowship (to W. E. Fowler) and research grant (to U. Aebi) and by National Institutes of Health Grant GM-27765 (to UA). U. Aebi is also the recipient of a research award from the Maurice-Muller-Foundation in Switzerland.

Received for publication 13 December 1982, and in revised form 22 March 1983.

REFERENCES

1. Aebi, U., W. E. Fowler, G. Isenberg, T. D. Pollard, and P. R. Smith. 1981. Crystalline actin sheets: their structure and polymorphism. *J. Cell Biol.* 91:340–351.
2. Smith, P. R., W. E. Fowler, T. D. Pollard, and U. Aebi. 1983. A three-dimensional model of the actin molecule determined by electron microscopy. *J. Mol. Biol.* In press.
3. Suck, D., W. Kabsch, and H. Mannherz. 1981. The three-dimensional structure of the skeletal muscle-bovine pancreatic DNase I complex at 6 angstroms. *Proc. Natl. Acad. Sci. USA.* 78:4319–4323.
4. Moore, P., H. Huxley, and D. J. DeRosier. 1970. Three-dimensional reconstruction of F-actin, thin filaments and decorated thin filaments. *J. Mol. Biol.* 50:279–295.
5. Spudich, J., H. Huxley, and J. Finch. 1972. Regulation of skeletal muscle contraction. II. Structural studies of the interaction of the tropomyosin-troponin complex with actin. *J. Mol. Biol.* 72:619–632.
6. Wakabayashi, T., H. Huxley, L. Amos, and A. Klug. 1975. Three-dimensional image reconstruction of actin-tropomyosin complex and actin-tropomyosin troponin T-troponin I complex. *J. Mol. Biol.* 93:477–497.
7. Egelman, E., and D. J. DeRosier. 1982. The structure of F-actin. *J. Cell Biol.* 95(2, Pt. 2):288*a*. (Abstr.)
8. Egelman, E., and D. J. DeRosier. 1983. The structure of F-actin. II. The shape and orientation of the subunit in the helix. *J. Mol. Biol.* In press.
9. Hanson, J., and J. Lowy. 1963. The structure of F-actin and of actin filaments isolated from muscle. *J. Mol. Biol.* 6:46–60.
10. DeRosier, D. J., and R. Censullo. 1981. Structure of F-actin from extracts of sea urchin oocytes. *J. Mol. Biol.* 146:77–99.
11. Ruben, G., N. Allen, and J. Travis. 1981. Structure of freeze-fractured, deep-etched F-actin. *Proceedings of the Thirty-ninth Annual EMSA Meeting.* 422–423.
12. Heuser, J., and M. Kirschner. 1980. Filament organization in platinum replicas of freeze-dried cytoskeletons. *J. Cell Biol.* 86:212–234.
13. Heuser, J. 1983. A procedure for freeze-drying molecules adsorbed to mica flakes. *J. Mol. Biol.* In press.
14. Smith, P. R. 1980. Freeze-drying specimens for electron microscopy. *J. Ultrastruct. Res.* 72:380–384.
15. Wrigley, N. 1968. The lattice spacing of crystalline catalase as an internal standard of length in electron microscopy. *J. Ultrastruct. Res.* 24:454–464.
16. Depue, R., and R. Rice. 1965. F-actin is a right-handed helix. *J. Mol. Biol.* 12:302–303.
17. Kellenberger, E., and J. Kistler. 1980. The physics of specimen preparation. *In* Unconventional Electron Microscopy for Molecular Structure Determination. W. Hoppe and R. Mason, editors). Friedr. Vieweg and Son, Braunschweig, Germany. 49–79.
18. Unwin, P. N. T. 1974. Electron microscopy of the stacked disk aggregate of Tobacco Mosaic Virus protein. II. The influence of electron irradiation on the stain distribution. *J. Mol. Biol.* 87:657–670.
19. Egelman, E., N. Francis, and D. J. DeRosier. 1982. F-actin is a helix with a random variable twist. *Nature (Lond.).* 298:131–135.
20. Kistler, J., U. Aebi, and E. Kellenberger. 1977. Freeze-drying and shadowing a two-dimensional periodic specimen. *J. Ultrastruct. Res.* 59:76–86.
21. Neugebauer, D.-C., and H. P. Zingsheim. 1979. Apparent holes in rotary shadowed proteins: dependence on angle of shadowing and replica thickness. *J. Microsc. (Oxf.).* 117:313–315.
22. Abermann, R., M. Salpeter, and L. Bachmann. 1972. High resolution shadowing. *In* Principles and Techniques of Electron Microscopy. M. Hayat, editor. 2:196–217.
23. Fowler, W. E., and U. Aebi. 1982. Polymorphism of actin paracrystals induced by polylysine. *J. Cell Biol.* 93:452–458.
24. DeRosier, D., E. Mandlekow, A. Silliman, L. Tilney, and R. Kane. 1977. Structure of actin-containing filaments from two types of non-muscle cells. *J. Mol. Biol.* 113:679–695.
25. Hartt, J., and R. Mendelson. 1980. X-ray scattering of F-actin and myosin subfragment-1 complex. *Fed. Proc.* 39:1728.
26. Matsudaira, P., E. Mandelkow, W. Renner, L. Hesterberg, and K. Weber. 1983. Role of fimbrin and villin in determining the interfilament distances of actin bundles. *Nature (Lond.).* 301:209–214.
27. Sakabe, N., K. Sakabe, K. Sasaki, H. Kondo, T. Ema, N. Kamiya, and M. Matsushima. 1983. Crystallographic studies of the chicken gizzard G-actin·DNase I complex at 5 Å resolution. *J. Biochem. (Tokyo).* 93:299–302.
28. Fowler, W. E., and U. Aebi. 1983. Preparation of single molecules and supramolecular complexes for high-resolution metal shadowing. *J. Ultrastruct. Res.* In press.